Geomechanics and Engineering, *Vol. 7, No. 5 (2014) 569-587*
DOI: http://dx.doi.org/10.12989/gae.2014.7.5.569

Creep properties and damage model for salt rock under low-frequency cyclic loading

Jun-Bao Wang [*1,2], Xin-Rong Liu [1,2] Xiao-Jun Liu [1] and Ming Huang [3]

[1] *School of Civil Engineering, Xi'an University of Architecture and Technology, Xi'an, China*
[2] *School of Civil Engineering, Chongqing University, Chongqing, China*
[3] *School of Civil Engineering, Fuzhou University, Fuzhou, China*

(*Received May 23, 2014, Revised July 13, 2014, Accepted August 06, 2014*)

Abstract. Triaxial compression creep tests were performed on salt rock samples using cyclic confining pressure with a static axial pressure. The test results show that, up to a certain time, changes in the confining pressure have little influence on creep properties of salt rock, and the axial creep curve is smooth. After this point, the axial creep curve clearly fluctuates with the confining pressure, and is approximately a straight line both when the confining pressure decreases and when it increases within one cycle period. The slope of these lines differs: it is greater when the confining pressure decreases than when it increases. In accordance with rheology model theory, axial creep equations were deduced for Maxwell and Kelvin models under cyclic loading. These were combined to establish an axial creep equation for the Burgers model. We supposed that damage evolution follows an exponential law during creep process and replaced the apparent stress in creep equation for the Burgers model with the effective stress, the axial creep damage equation for the Burgers model was obtained. The model suitability was verified using creep test results for salt rock. The fitting curves are in excellent agreement with the test curves, so the proposed model can well reflect the creep behavior of salt rock under low-frequency cyclic loading. In particular, it reflects the fluctuations in creep deformation and creep rate as the confining pressure increasing and decreasing under different cycle periods.

Keywords: salt rock; creep properties; low-frequency cyclic loading; damage model; fluctuation

1. Introduction

Salt rock is a soft rock with a number of advantages such as a compact structure, low permeability, mechanical stability, and a strong ability to self-recover from damage, so it is recognized as the perfect medium for underground storage of natural gas, crude oil and compressed air, and for underground disposal of CO_2 and high-level radioactive waste (Wang *et al*. 2013, Liang *et al*. 2007, 2011, Chan *et al*. 1996, Yang *et al*. 2013, Guo *et al*. 2012, Wang *et al*. 2011). Creep property is one of the most important mechanical properties of salt rock and is a key factor in the long-term stability and safety of salt rock underground cavities (Weidinger *et al*. 1997, Ślizowski and Lankof 2003).

Many efforts have been directed toward the study on creep properties of salt rock in recent

*Corresponding author, Lecturer, E-mail: xajdwangjunbao@163.com

http://www.techno-press.org/?journal=gae&subpage=7 ISSN: 2005-307X (Print), 2092-6219 (Online)

years because of the importance of salt rock in underground storage of energies. Yang *et al*. (1999) carried out a number of uniaxial and triaxial creep tests, and suggested an exponential function to characterize the creep strain from transient to steady-state creep of salt rock considering the effects of confining pressure and axial pressure on the time-dependent stress-strain behavior. Asanov and Pan'kov (2004) studied the shear creep properties of salt rock. Zhang *et al*. (2012) conducted triaxial creep tests to the glauberite, anhydrite, and argillaceous salt rock, which investigated the strain rate of argillaceous salt rock is lower than glauberite and anhydrite salt rock, and the difference becomes larger with the increase of deviatoric stress. Dubey and Gairola (2008) investigated the influence of structural anisotropy on time-dependent deformation (creep) of rock salt. Chan *et al*. (1994, 1997) proposed a Multimechanism Deformation Coupled Fracture (MDCF) model of salt rock by incorporating continuum, isotropic damage as a fully coupled variable that enhanced the stress influence by reduction of the effective area and contributed directly to the inelastic strain rate. In this MDCF model, the mechanisms of dislocation creep, shear creep, tensile damage, damage healing etc can be considered. But it is quite complex and not convenient to use. Heusermann *et al*. (2003) used the LUBBY2 constitutive model to describe the nonlinear creep behavior of rock salt. Jin and Cristescu (1998) developed a new viscoplastic constitutive model for transient creep of salt rock, and the new constitutive model was employed by the authors to analyze the stress distribution around a plane strain borehole excavated in salt rock neglecting the effect of large deformation and steady state creep. Munson (1997) suggested a multimechanism constitutive model of the creep of polycrystalline salt rock based on steady state creep as modified to incorporate transient creep through workhardening and recovery. Yahya *et al*. (2000) constructed a unified viscoplastic model with a single set of equations and material constants for describing both short term and long term ductile behavior of rock salt. Nazary Moghadam *et al*. (2013) formulated a numerical model of the time-dependent behavior of underground caverns excavated in salt rock, and used the new model to describe dilatancy, short-term failure as well as long-term failure during transient and steady state creep of salt rock. On the basis of time-based fractional derivative, Zhou *et al*. (2011, 2012, 2013) constructed creep constitutive model by replacing a Newtonian dashpot in the classical Nishihara model with the fractional derivative Abel dashpot, and the time-based fractional derivative model can be simplified to the Nishihara model for the special case of fractional derivative order equal to 1.

However, most of the studies cited above are on the creep properties of salt rock under static loading, and there have been few studies on creep properties under cyclic loading. During long-term service of underground storage, the deformation process for the surrounding rock mass is a creep process under the action of cyclic loading due to periodic injection and production characteristics of salt rock storage, which results in periodic fluctuations in cavern pressure. Therefore, it is of practical engineering significance to research the creep properties of salt rock under the action of cyclic loading.

In this study, triaxial compression creep tests were conducted under the action of low-frequency cyclic loading (ignoring the fatigue effect) on salt rock samples using stress loading involving cyclic confining pressure and static axial pressure. Low-frequency cyclic loading was chosen because of the relatively long injection–production cycle period during gas storage service and the relatively low number of cycles during its service life (Chen *et al*. 2007). Therefore, we supposed that low-frequency cyclic loading occurs and ignored the fatigue effect for salt rock. The creep deformation properties of salt rock under low-frequency cyclic loading were analyzed according to the test results. Then, a creep damage model for salt rock under low-frequency cyclic loading was established on the basis of rheology model and damage mechanics theories, and the

suitability of which was verified using the test results.

2. Materials and methods

2.1 Sample preparation

Salt rock samples were obtained from a salt mine in Huai'an (Jiangsu Province, China). This salt unit is considered as host rock for natural gas storage. The samples are relatively pure halite with slight amounts (< 5%) of insoluble materials (argillaceous, anhydrite, and glauberite) and have a natural density of approximately 2.2 g/cm^3. The samples were prepared as cylinders with a diameter of 50 mm and a height of 100 mm, according to the International Society for Rock Mechanics (ISRM).

2.2 Test equipment

Creep tests were performed using an RLW-2000 rheology testing system that comprises axial loading, confining pressure loading, numerical control, and measurement systems. It is suitable for uniaxial compression, triaxial compression, creep, relaxation, seepage, and cyclic loading tests. The maximum axial load is 2000 kN and the measurement resolution is 200 N; the maximum confining pressure is 60 MPa and the measurement resolution is 0.001 MPa.

2.3 Test program

Triaxial compression creep tests were performed under the action of low-frequency cyclic loading (ignoring the fatigue effect) on two salt rock samples using the stress-loading mode of cyclic confining pressure with static axial pressure. The cyclic confining pressure takes the form of a triangular wave and the stress loading mode is shown in Fig. 1.

The axial stress for both samples was σ_1 = 25 MPa, the maximum confining pressure was σ_{3max} = 20 MPa, and the minimum confining pressure was σ_{3min} = 10 MPa. The cycle period for the confining pressure, T_0, was varied. Low-frequency cyclic loading was chosen because of the

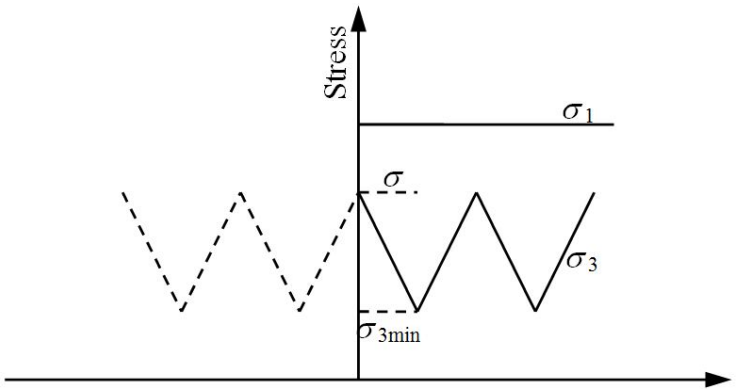

Fig. 1 Stress loading mode for salt rock creep tests

Table 1 Load parameters for salt rock creep tests

Sample	Axial pressure (MPa)	Confining pressure		
		σ_{3max} (MPa)	σ_{3min} (MPa)	T_0 (h)
SR1	25	20	10	4
SR2	25	20	10	8

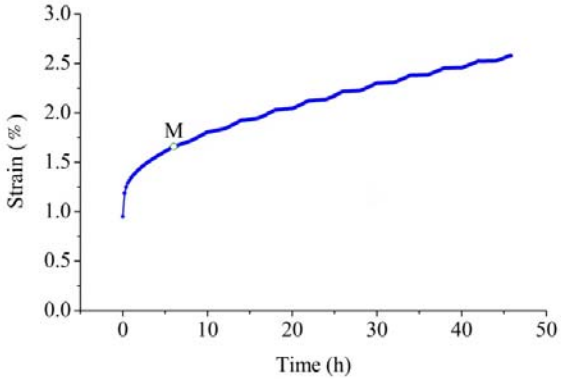

(a) SR1 sample

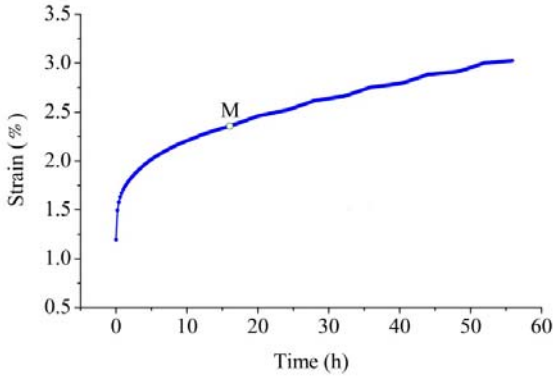

(b) SR2 sample

Fig. 2 Axial creep curves for salt rock under cyclic loading: (a) SR1 sample; and (b) SR2 sample

relatively long injection–production cycle period during gas storage service and the relatively low number of cycles during its service life (Chen *et al*. 2007). Therefore, we assumed that low-frequency cyclic loading occurs and ignored the fatigue effect for salt rock. In addition, limited by the test conditions, the test cannot last too long. On the basis of these considerations, cycle periods for confining pressure for the two samples were determined as T_0 = 4 h and T_0 = 8 h, respectively. Table 1 lists the parameters for the loading program.

2.4 Test procedure

Before testing, the salt rock samples were covered with heat-shrinkable rubber to make them

oil-proofed. The rubber cover was heated with a high-power hair drier to shrink it so that it adhered to the sample surface. The sealed samples were then placed at the center of a triaxial cell of the rheology testing system so that the sample's axis coincided with the loading center line of the testing machine to avoid eccentric compression. The initial values of the axial pressure and confining pressure were set and applied at a certain loading rate. The measurement was started to record once the axial pressure and confining pressure reached the initial values. The ambient temperature was kept at 25 ± 1°C throughout the test process.

3. Test results

No radial creep curves were obtained during the test process because of a radial sensor malfunction, so only axial creep curves were obtained (see Figs. 2(a)-(b)). Figs. 2(a)-(b) reveal that salt rock samples exhibit significant time-dependent deformation, but no accelerated creep stage occurs. Two possible reasons are as follows: (1) the rheological test machine used in the test has its measuring range. In order to prevent the creep deformation of the salt rock from exceeding the effective range of the machine, relatively smaller deviatoric stresses were applied to the samples

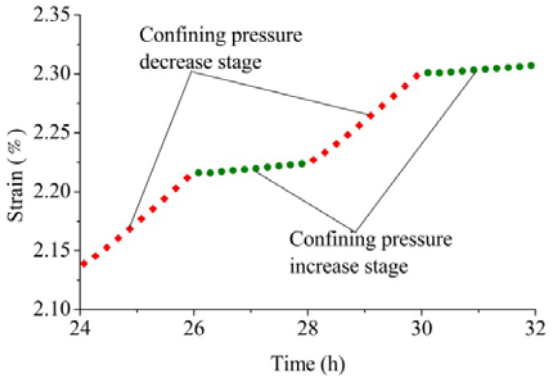

(a) SR1 sample

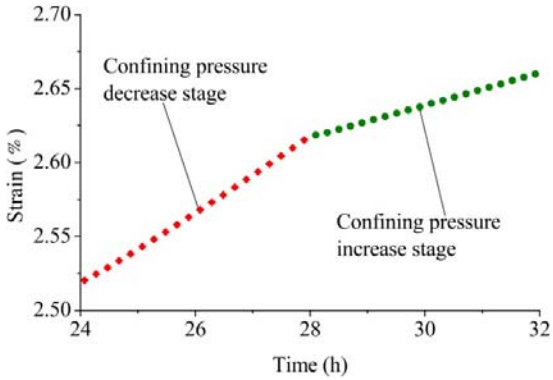

(b) SR2 sample

Fig. 3 Axial creep curves from 24 to 32 h: (a) SR1 sample; and (b) SR2 sample

during the test; and (2) limited by the laboratory conditions, the creep test didn't last long enough.

Within a certain time (point "*M*" in Figs. 2(a)-(b), ~6 h for sample SR1 and ~16 h for SR2), creep deformation rapidly increases with time, but the creep rate gradually decreases. In this stage, the effect of confining pressure on the salt rock creep properties is small and the axial creep curve is smooth. After this time, changes in the confining pressure gradually affect the sample creep and the axial creep curve clearly fluctuates with the confining pressure. This fluctuation is more pronounced for sample SR1 than for SR2. Thus, the smaller the cycle period for the confining pressure is, the more distinct are the axial creep fluctuations.

To observe creep fluctuations under the action of cyclic loading more clearly, Figs. 3(a)-(b) show the creep curves from 24 to 32 h. It is evident see that within one confining pressure cycle, the creep curve is approximately a straight line both when the confining pressure decreases and when it increases. However, the slope of these straight lines differs and is greater when the confining pressure decreases than when it increases. This indicates that creep rate for salt rock is greater when the confining pressure decreases than when it increases under cyclic loading. Thus, confining pressure has a great impact on the creep properties of salt rock. The slope of the straight lines both when the confining pressure decreases and when it increases gradually decreases as the

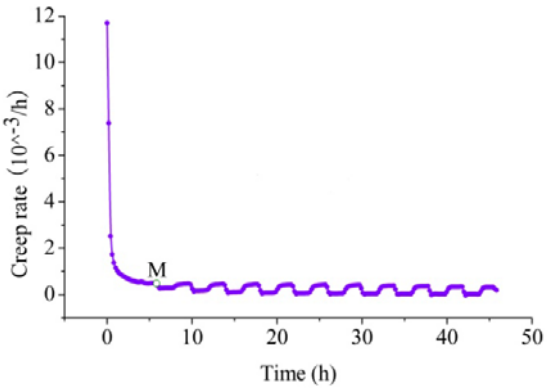

(a) SR1 sample

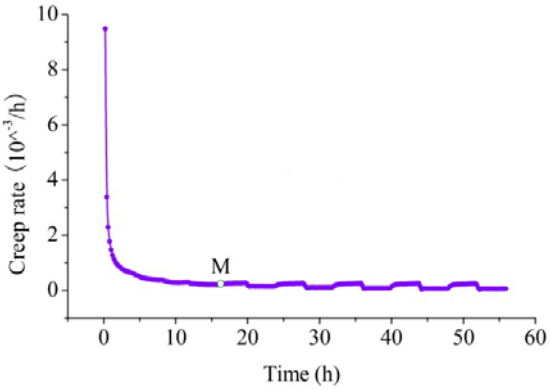

(b) SR2 sample

Fig. 4 Creep rate curves for salt rock under cyclic loading: (a) SR1 sample; and (b) SR2 sample

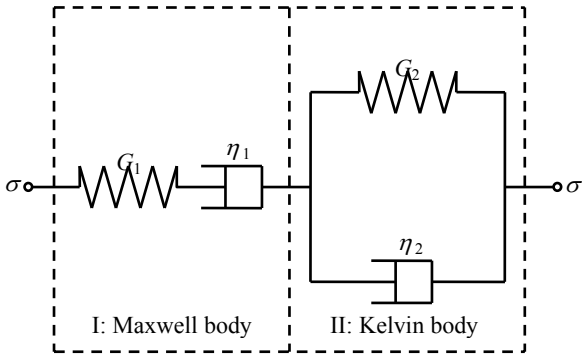

Fig. 5 Schematic view of the Burgers model

time and number of loading cycles increase, and reaches a stable minimum value after 40 h, respectively.

Figs. 4(a)-(b) show creep rate curves for the salt rock samples. The creep rate rapidly decreases and is hardly influenced by changes in the confining pressure up to point "*M*", and the creep rate curve is fairly smooth. After point "*M*", the creep rate curve is to a square wave, and the creep rate regularly fluctuates with increasing and decreasing confining pressure. The creep rate reaches to the maximum value when the confining pressure decreases and the minimum value when the confining pressure increases. This fluctuating wave pattern for the creep rate is more pronounced for sample SR1 than that for SR2.

4. Creep damage model

The creep curves for salt rock under cyclic loading in Figs. 2(a)-(b) are similar to the creep curve from the Burgers model (Chopra 1997, Zhang *et al*. 2012). However, the conventional Burgers model can only describe creep for materials under static loading and cannot reflect deformation fluctuations under cyclic loading. Therefore, we used the Burgers model in combination with damage mechanics theory to deduce the axial creep equation for salt rock under the action of low-frequency cyclic loading (ignoring the fatigue effect).

The Burgers model involves serial connection of Maxwell and Kelvin models, as shown in Fig. 5. According to Fig. 5, we have.

$$\begin{cases} \sigma(t) = \sigma^{\mathrm{M}}(t) = \sigma^{\mathrm{K}}(t) \\ \varepsilon(t) = \varepsilon^{\mathrm{M}}(t) + \varepsilon^{\mathrm{K}}(t) \end{cases} \tag{1}$$

where $\sigma(t)$, $\sigma^M(t)$, and $\sigma^K(t)$ are stress, and $\varepsilon(t)$, $\varepsilon^M(t)$, and $\varepsilon^K(t)$ are strain for the Burgers, Maxwell, and Kelvin models, respectively.

4.1 Expression for cyclic loading

To deduce the creep equation for salt rock under cyclic loading, an expression for the confining pressure as a function of time must be determined. To this end, the triangular wave for the

confining pressure must be expanded, as shown by the dotted line in Fig. 1. Thus, the confining pressure during one cycle can be expressed as

$$\sigma_3(t)=\begin{cases}\sigma_{3\max}+\dfrac{\sigma_{3\max}-\sigma_{3\min}}{T_0/2}t & \left(-\dfrac{T_0}{2}\le t<0\right)\\ \sigma_{3\max}-\dfrac{\sigma_{3\max}-\sigma_{3\min}}{T_0/2}t & \left(0\le t\le\dfrac{T_0}{2}\right)\end{cases} \tag{2}$$

where $\sigma_3(t)$ is the confining pressure, t is time, $\sigma_{3\max}$ is the maximum and $\sigma_{3\min}$ is the minimum confining pressure, and T_0 is the cycle period.

Since $\sigma_3(t)$ is an even function related to time t, according to trigonometric expansion, the constant component $a_0=(\sigma_{3\max}+\sigma_{3\min})/2$, the sinusoidal component amplitude $b_n=0$, and the cosine component amplitude is given by

$$a_n=\frac{2}{T_0}\int_{-T_0/2}^{T_0/2}\sigma_3(t)\cos n\omega_0 t dt=\frac{4}{T_0}\int_0^{\frac{T_0}{2}}\left(\sigma_{3\max}-\frac{\sigma_{3\max}-\sigma_{3\min}}{T_0/2}t\right)\cos n\omega_0 t dt \tag{3}$$

where n is a positive integer, ω_0 is the angular velocity, and $\omega_0=2\pi/T_0$.

Taking the integral of Eq. (3) with respect to time, we obtain

$$a_n=\frac{4(\sigma_{\max}-\sigma_{3\min})}{n^2\pi^2}\sin^2\frac{n\pi}{2} \tag{4}$$

namely

$$a_n=\begin{cases}\dfrac{4(\sigma_{3\max}-\sigma_{3\min})}{n^2\pi^2} & n=1,3,5,7\cdots L\\ 0 & n=2,4,6,8\cdots L+1\end{cases} \tag{5}$$

Then the expanded equation for $\sigma_3(t)$ is

$$\sigma_3(t)=\frac{\sigma_{3\max}+\sigma_{3\min}}{2}+\frac{4(\sigma_{3\max}-\sigma_{3\min})}{\pi^2}\left(\cos\omega_0 t+\frac{1}{3^2}\cos 3\omega_0 t+\frac{1}{5^2}\cos 5\omega_0 t+\cdots\right) \tag{6}$$

Eq. (6) contains an infinite series expansion, and in real applications the first several terms can be taken approximately according to the precision required. For easy calculation to the required precision, the first two terms are taken here, namely

$$\sigma_3(t)=\frac{\sigma_{3\max}+\sigma_{3\min}}{2}+\frac{4(\sigma_{3\max}-\sigma_{3\min})}{\pi^2}\left(\cos\omega_0 t+\frac{1}{9}\cos 3\omega_0 t\right) \tag{7}$$

Analyzing the extremum of Eq. (7), we find

$$\begin{cases}\sigma_{3\max}(t)=0.95\sigma_{3\max}+0.05\sigma_{3\min}\neq\sigma_{3\max}\\ \sigma_{3\min}(t)=0.95\sigma_{3\min}+0.05\sigma_{3\max}\neq\sigma_{3\min}\end{cases} \tag{8}$$

It is evident from Eq. (8) that owing to approximate treatment, Eq. (7) cannot precisely meet the max. and min. values of confining pressure. To satisfy the maximum and minimum confining pressure, Eq. (7) is amended as

$$\sigma_3(t) = \frac{\sigma_{3\max} + \sigma_{3\min}}{2} + \frac{4.4415(\sigma_{3\max} - \sigma_{3\min})}{\pi^2}\left(\cos\omega_0 t + \frac{1}{9}\cos 3\omega_0 t\right) \tag{9}$$

namely

$$\sigma_3(t) = 0.5(\sigma_{3\max} + \sigma_{3\min}) + 0.45(\sigma_{3\max} - \sigma_{3\min})\left(\cos\omega_0 t + \frac{1}{9}\cos 3\omega_0 t\right) \tag{10}$$

Although this is not theoretically rigorous, the boundary conditions for the confining pressure cycle can be met precisely.

The stress tensor σ_{ij} for a material under three-dimensional stress can be divided into the spherical stress tensor σ_m and the deviator stress tensor S_{ij} (Zhang *et al*. 2011). It is generally recognized that σ_m can only change the bulk of the material, while S_{ij} can only change its shape. The relationship between σ_{ij}, σ_m, and S_{ij} is given by

$$\begin{cases} \sigma_m = \dfrac{\sigma_1 + \sigma_2 + \sigma_3}{3} \\ S_{ij} = \sigma_{ij} - \sigma_m \delta_{ij} \end{cases} \tag{11}$$

where σ_1, σ_2, and σ_3 are principal stresses in the three directions and δ_{ij} is the Kronecker function.

In the case of conventional triaxial compression, because of lateral stress ($\sigma_2 = \sigma_3$), axial deviatoric stress can be expressed as

$$S_{11}(t) = \frac{2[\sigma_1 - \sigma_3(t)]}{3} \tag{12}$$

Substituting Eq. (10) into Eq. (12), we have

$$S_{11}(t) = \frac{2}{3}\left[\sigma_1 - 0.5(\sigma_{3\max} + \sigma_{3\min}) - 0.45(\sigma_{3\max} - \sigma_{3\min})\left(\cos\omega_0 t + \frac{1}{9}\cos 3\omega_0 t\right)\right] \tag{13}$$

4.2 Axial creep equation for the Maxwell model under cyclic loading

The Maxwell model comprises a Hooke body and a Newton body connected in series (Fig. 5) for which the constitutive equation is (Zhang *et al*. 2011)

$$\frac{de_{ij}^M(t)}{dt} = \frac{1}{2G_1}\frac{dS_{ij}^M(t)}{dt} + \frac{S_{ij}^M(t)}{2\eta_1} \tag{14}$$

where $e_{ij}^M(t)$ is the deviator strain tensor, $S_{ij}^M(t)$ is the deviator stress tensor, G_1 is the shear modulus, and η_1 is the viscosity coefficient.

Taking the derivative of Eq. (13) with respect to time, the rate of change in $S_{11}(t)$ can be obtained as

$$\frac{dS_{11}(t)}{dt}=\frac{2}{3}\times 0.45(\sigma_{3\max}-\sigma_{3\min})\omega_0\left(\sin\omega_0 t+\frac{1}{3}\sin 3\omega_0 t\right) \tag{15}$$

From Eq. (1) we know that $S_{11}^{M}(t)=S_{11}(t)$. By substituting Eqs. (13) and (15) into Eq. (14), we obtain the relation between axial deviator stress and axial deviator strain for the Maxwell model under the cyclic loading shown in Fig. 1 as

$$\begin{aligned}\frac{de_{11}^{M}(t)}{dt}=&\frac{\sigma_1-0.5(\sigma_{3\max}+\sigma_{3\min})}{3\eta_1}+\frac{0.45(\sigma_{3\max}-\sigma_{3\min})\omega_0}{3G_1}\sin\omega_0 t\\&-\frac{0.45(\sigma_{3\max}-\sigma_{3\min})}{3\eta_1}\cos\omega_0 t+\frac{0.45(\sigma_{3\max}-\sigma_{3\min})\omega_0}{9G_1}\sin 3\omega_0 t\\&-\frac{0.45(\sigma_{3\max}-\sigma_{3\min})}{27\eta_1}\cos 3\omega_0 t\end{aligned} \tag{16}$$

Taking the integral of Eq. (16) with respect to time, we obtain

$$\begin{aligned}e_{11}^{\mathrm{M}}(t)=&\frac{\sigma_1-0.5(\sigma_{3\max}+\sigma_{3\min})}{3\eta_1}t-0.45(\sigma_{3\max}-\sigma_{3\min})A_{\mathrm{M1}}\sin(\omega_0 t+A_{\mathrm{M}})\\&-0.45(\sigma_{3\max}-\sigma_{3\min})B_{\mathrm{M1}}\sin(3\omega_0 t+B_{\mathrm{M}})+C_0\end{aligned} \tag{17}$$

where C_0 is the integration constant and

$$\begin{cases}A_{\mathrm{M1}}=\sqrt{\dfrac{1}{(3\eta_1\omega_0)^2}+\dfrac{1}{9G_1^2}}\\[2ex] B_{\mathrm{M1}}=\sqrt{\dfrac{1}{(81\eta_1\omega_0)^2}+\dfrac{1}{(27G_1)^2}}\end{cases} \tag{18}$$

$$\begin{cases}A_{\mathrm{M}}=\arccos\dfrac{1}{3\eta_1\omega_0 A_{\mathrm{M1}}}\\[2ex] B_{\mathrm{M}}=\arccos\dfrac{1}{81\eta_1\omega_0 B_{\mathrm{M1}}}\end{cases} \tag{19}$$

According to Eq. (10), $\sigma_3(t)=\sigma_{3\max}$ when $t=0$. At this instant, $e_{11}^{M}=(\sigma_1-\sigma_{3\max})/3G_1$. Substituting this initial condition into Eq. (17), C_0 can be determined as

$$C_0=\frac{\sigma_1-\sigma_{3\max}}{3G_1}+0.45(\sigma_{3\max}-\sigma_{3\min})(A_{M1}\sin A_M+B_{M1}\sin B_M) \tag{20}$$

Substituting Eq. (20) into Eq. (17), we obtain

$$\begin{aligned} e_{11}^{M}(t) = & \frac{\sigma_1 - \sigma_{3\max}}{3G_1} + \frac{\sigma_1 - 0.5(\sigma_{3\max} + \sigma_{3\min})}{3\eta_1} t \\ & + 0.45(\sigma_{3\max} - \sigma_{3\min}) A_{M1} \left[\sin A_M - \sin(\omega_0 t + A_M)\right] \\ & + 0.45(\sigma_{3\max} - \sigma_{3\min}) B_{\mathrm{M1}} \left[\sin B_M - \sin(3\omega_0 t + B_{\mathrm{M}})\right] \end{aligned} \tag{21}$$

Thus, the axial deviator strain for Maxwell model produced by axial deviator stress can be determined.

According to the generalized Hooke's law, the constitutive relation for a Hooke body under three-dimensional stress is given by (Yahya *et al*. 2000)

$$\begin{cases} \sigma_m = 3K\varepsilon_m \\ S_{ij} = 2Ge_{ij} \end{cases} \tag{22}$$

where σ_m is the spherical stress tensor, ε_m is the spherical strain tensor, K is the bulk modulus, and G is the shear modulus, with

$$\begin{cases} K = \dfrac{E}{3(1-2\nu)} \\ G = \dfrac{E}{2(1+\nu)} \end{cases} \tag{23}$$

where E is the elastic modulus and v is Poisson's ratio.

If the influence of the changing load on ε_m is not taken into account and ε_m is calculated for the load at $t = 0$, according to Eq. (22) we have

$$\varepsilon_{\mathrm{m}} = \frac{\sigma_{\mathrm{m}}}{3K} = \frac{\sigma_1 + 2\sigma_{3\max}}{9K} \tag{24}$$

Combining Eq. (21) with Eq. (24), the axial creep equation for the Maxwell model under the low-frequency cyclic loading shown in Fig. 1 can be expressed as

$$\begin{aligned} \varepsilon_{11}^{M}(t) = & \frac{\sigma_1 + 2\sigma_{3\max}}{9K} + \frac{\sigma_1 - \sigma_{3\max}}{3G_1} + \frac{\sigma_1 - 0.5(\sigma_{3\max} + \sigma_{3\min})}{3\eta_1} t \\ & + 0.45(\sigma_{3\max} - \sigma_{3\min}) A_{M1} \cdot \left[\sin A_M - \sin(\omega_0 t + A_M)\right] \\ & + 0.45(\sigma_{3\max} - \sigma_{3\min}) B_{M1} \left[\sin B_M - \sin(3\omega_0 t + B_{\mathrm{M}})\right] \end{aligned} \tag{25}$$

4.3 Axial creep equation for the Kelvin model under cyclic loading

The Kelvin model comprises a Hooke body and a Newton body connected in parallel (Fig. 5), for which the constitutive equation is expressed as (Zhang *et al*. 2011)

$$S_{ij}^K(t) = 2G_2 e_{ij}^K(t) + 2\eta_2 \frac{de_{ij}^K(t)}{\mathrm{d}t} \tag{26}$$

where $e_{ij}^K(t)$ is the deviator strain tensor, $S_{ij}^K(t)$ is the deviator stress tensor, G_2 is the shear modulus, and η_2 is the viscosity coefficient.

Eq. (26) can be rewritten as

$$\frac{de_{ij}^K(t)}{dt} + \frac{G_2}{\eta_2} e_{ij}^K(t) = \frac{S_{ij}^K(t)}{2\eta_2} \tag{27}$$

According to Eq. (1), we know that $S_{11}^K(t) = S_{11}(t)$. Substituting Eq. (13) into Eq. (27), the relation between axial deviator stress and axial deviator strain for the Kelvin model under the cyclic loading shown in Fig. 1 is obtained as

$$\begin{aligned} &\frac{de_{11}^K(t)}{dt} + \frac{G_2}{\eta_2} e_{11}^K(t) \\ &= \frac{1}{3\eta_2}\left[\sigma_1 - 0.5(\sigma_{3\max} + \sigma_{3\min}) - 0.45(\sigma_{3\max} - \sigma_{3\min})\left(\cos\omega_0 t + \frac{1}{9}\cos 3\omega_0 t\right)\right] \end{aligned} \tag{28}$$

Solving this differential equation, we obtain

$$\begin{aligned} e_{11}^K(t) = {} & \frac{\sigma_1 - 0.5(\sigma_{3\max} + \sigma_{3\min})}{3G_2} - 0.45(\sigma_{3\max} - \sigma_{3\min}) A_{K1} \sin(\omega_0 t + A_K) \\ & - 0.45(\sigma_{3\max} - \sigma_{3\min}) B_{K1} \sin(3\omega_0 t + B_K) + C_0 \exp\left(-\frac{G_2}{\eta_2} t\right) \end{aligned} \tag{29}$$

where C_0 is the integration constant and

$$\begin{cases} A_{K1} = \dfrac{1}{3\sqrt{G_2^2 + \eta_2^2\omega_0^2}} \\ B_{K1} = \dfrac{1}{27\sqrt{G_2^2 + 9\eta_2^2\omega_0^2}} \end{cases} \tag{30}$$

$$\begin{cases} A_K = \arccos 3A_{K1}\eta_2\omega_0 \\ B_K = \arccos 81B_{K1}\eta_2\omega_0 \end{cases} \tag{31}$$

For the Kelvin model, $e_{11}^K = 0$ when $t = 0$. Considering this initial condition, C_0 is determined as

$$C_0 = 0.45(\sigma_{3\max} - \sigma_{3\min})(A_{K1}\sin A_K + B_{K1}\sin B_K) - \frac{\sigma_1 - 0.5(\sigma_{3\max} + \sigma_{3\min})}{3G_2} \tag{32}$$

Substituting Eq. (32) into Eq. (29), we obtain

$$
\begin{aligned}
e_{11}^{K}(t) = {} & \frac{\sigma_1 - 0.5(\sigma_{3\max} + \sigma_{3\min})}{3G_2}\left[1 - \exp\left(-\frac{G_2}{\eta_2}t\right)\right] \\
& + 0.45(\sigma_{3\max} - \sigma_{3\min})A_{K1}\left[\sin A_K \exp\left(-\frac{G_2}{\eta_2}t\right) - \sin(\omega_0 t + A_K)\right] \\
& + 0.45(\sigma_{3\max} - \sigma_{3\min})B_{K1}\left[\sin B_K \exp\left(-\frac{G_2}{\eta_2}t\right) - \sin(3\omega_0 t + B_K)\right]
\end{aligned} \tag{33}
$$

Analysis reveals that the curve described by the first term in Eq. (33) is the creep curve for the Kelvin model under static loading with axial pressure of σ_1 and confining pressure of $0.5(\sigma_{3\max} + \sigma_{3\min})$, while the curves described by both the second and third terms fluctuate according to a wave pattern.

The Kelvin model is normally used to describe the primary creep property of material. According to the results for salt rock under cyclic loading as shown in Fig. 2, changes in the confining pressure have a small effect on creep, and fluctuations in the creep curve are not significant up to a certain time as well. Thus, to simplify the calculation, we can consider that the failure of salt rock is controlled by deformation, and let $\sin(\omega_0 t + A_K) = \sin(3\omega_0 t + B_K) \equiv -1$. Furthermore, because there is no spherical strain, the axial strain of the Kelvin model is $\varepsilon_{11}^{K} = e_{11}^{K}$.

Based on the above analysis, Eq. (33) can be written as

$$
\begin{aligned}
\varepsilon_{11}^{K} = {} & \frac{\sigma_1 - 0.5(\sigma_{3\max} + \sigma_{3\min})}{3G_2}\left[1 - \exp\left(-\frac{G_2}{\eta_2}t\right)\right] \\
& + 0.45(\sigma_{3\max} - \sigma_{3\min})A_{K1}\left[\sin A_K \exp\left(-\frac{G_2}{\eta_2}t\right) + 1\right] \\
& + 0.45(\sigma_{3\max} - \sigma_{3\min})B_{K1}\left[\sin B_K \exp\left(-\frac{G_2}{\eta_2}t\right) + 1\right]
\end{aligned} \tag{34}
$$

4.4 Axial creep damage equation for the Burgers model under cyclic loading

The Burgers model comprises a Maxwell model and a Kelvin model connected in series. Thus, combining Eqs. (1), (25), and (34), the axial creep equation for the Burgers model under the cyclic loading shown in Fig. 1 can be expressed as

$$
\begin{aligned}
\varepsilon_{11} = {} & \frac{\sigma_1 + 2\sigma_{3\max}}{9K} + \frac{\sigma_1 - \sigma_{3\max}}{3G_1} + \frac{\sigma_1 - 0.5(\sigma_{3\max} + \sigma_{3\min})}{3\eta_1}t \\
& + 0.45(\sigma_{3\max} - \sigma_{3\min})\left\{A_{M1}\left[\sin A_M - \sin(\omega_0 t + A_M)\right] + B_{M1}\left[\sin B_M - \sin(3\omega_0 t + B_M)\right]\right\} \\
& + \frac{\sigma_1 - 0.5(\sigma_{3\max} + \sigma_{3\min})}{3G_2}\left[1 - \exp\left(-\frac{G_2}{\eta_2}t\right)\right] \\
& + 0.45(\sigma_{3\max} - \sigma_{3\min})\left\{A_{K1}\left[\sin A_K \exp\left(-\frac{G_2}{\eta_2}t\right) + 1\right] + B_{K1}\left[\sin B_K \exp\left(-\frac{G_2}{\eta_2}t\right) + 1\right]\right\}
\end{aligned} \tag{35}
$$

According to the test results, salt rock exhibits distinct creep deformation under an applied load. Based on the rheological damage theory, new fissures within a material will be continuously produced by creep deformation. These fissures will gradually expand over time, resulting in degradation of the mechanical properties and a decrease in strength.

According to the classic damage mechanics, damage evolution for a material can be expressed in terms of the effective bearing area $\widetilde{S}$ as

$$D = 1 - \frac{\widetilde{S}}{S} \tag{36}$$

where S is the total area and D is the damage factor, $0 \le D \le 1$.

The effective stress $\widetilde{\sigma}$ borne by the material can thus be written as

$$\widetilde{\sigma} = \frac{\sigma}{1-D} \tag{37}$$

where σ is the apparent or Cauchy stress. The apparent stress and effective stress can only be equal when $D = 0$.

An appropriate damage evolution equation needs to be determined to establish a creep model according to the mechanical damage method. In accordance with the results reported by Jiang *et al*. (2011), the damage evolution equation can be determined in exponential form as

$$D(t) = 1 - \exp(-t^n) \tag{38}$$

where n is a constant related to the rock properties.

Substituting Eq. (38) into Eq. (37), we obtain

$$\widetilde{\sigma} = \sigma \exp(t^n) \tag{39}$$

We assume that salt rock is an isotropic material and the damage is also isotropic. According to the strain equivalent principle (Lemaitre 1984), replacing the apparent stress in Eq. (35) by the effective stress expressed by Eq. (39), we can obtain

$$\begin{aligned}
\varepsilon_{11} = \Bigg\{ & \frac{\sigma_1 + 2\sigma_{3\max}}{9K} + \frac{\sigma_1 - \sigma_{3\max}}{3G_1} + \frac{\sigma_1 - 0.5(\sigma_{3\max} + \sigma_{3\min})}{3\eta_1} t \\
& + 0.45(\sigma_{3\max} - \sigma_{3\min})\left\{A_{M1}\left[\sin A_M - \sin(\omega_0 t + A_M)\right] + B_{M1}\left[\sin B_M - \sin(3\omega_0 t + B_M)\right]\right\} \\
& + \frac{\sigma_1 - 0.5(\sigma_{3\max} + \sigma_{3\min})}{3G_2}\left[1 - \exp\left(-\frac{G_2}{\eta_2} t\right)\right] \\
& + 0.45(\sigma_{3\max} - \sigma_{3\min})\left\{A_{K1}\left[\sin A_K \exp\left(-\frac{G_2}{\eta_2} t\right) + 1\right]\right. \\
& \left. + B_{K1}\left[\sin B_K \exp\left(-\frac{G_2}{\eta_2} t\right) + 1\right]\right\}\Bigg\} \exp(t^n)
\end{aligned} \tag{40}$$

Eq. (40) can be used as the axial creep damage equation for the Burgers model under cyclic loading shown in Fig. 1.

5. Model verification

The suitability of Eq. (40) was evaluated using creep results for salt rock under low-frequency cyclic loading. Firstly, based on the nonlinear least-squares theory, creep parameters were determined using the curve-fitting method (Yang and Cheng 2011) and 1stOpt mathematical optimization software. The greatest advantage of the software is that the software will give initial values of the parameters to be determined instead of inputting them by users, and can determine the globally optimal solution by the special method of universal global optimization. The fitting method and steps are as follows:

(I) Eq. (40) is compiled into the fitting code for software identification in the form of self-defining function.

(II) The creep parameters to be inversed are taken as the design variable, namely

$$X = \{E,\ G_2,\ \eta_1,\ \eta_2,\ n\} \tag{41}$$

where E is the elastic modulus of salt rock. When E is obtained, the bulk modulus K and shear modulus G_1 can be determined according to Eq. (23) and the Poisson′s ratio for salt rock $v = 0.3$.

(III) The target function

$$Q = \sum_{i=1}^{N} \left[w_i(\boldsymbol{X}, t_i) - w_i \right]^2 \tag{42}$$

is constructed, where N is the number of test data groups, $w_i(X, t_i)$ is the strain calculated at time t_i, w_i is the strain measured at time t_i, and Q is the target function, namely the error-squared sum.

(IV) The precision is set for the target function Q and iteration is carried out to obtain a solution. If the value of Q calculated satisfies the precision requirement, iteration ceases and the calculated results are outputted; if not, iteration continues till the precision requirement is satisfied.

Table 2 lists the inversion results for salt rock creep parameters. Figs. 6(a)-(b) compare fitting and experimental creep curves, while Figs. 7(a)-(b) compare fitting and experimental creep rate curves.

According to the data in Table 2, the correlation coefficient $R > 0.99$ for both samples, this indicates that the fitting parameters are highly correlated. Figs. 6(a)-(b) and 7(a)-(b) reveal that

Table 2 Inversion results for the creep parameters

Samples	Cycle period (h)	Parameters						R
		K (MPa)	G_1 (MPa)	G_2 (MPa)	η_1 (MPa·h)	η_2 (MPa·h)	n	
SR1	4	93 043	42 943	1 027	114 682	169	0.091	0.992
SR2	8	126 179	58 237	788	151 665	215	0.081	0.991

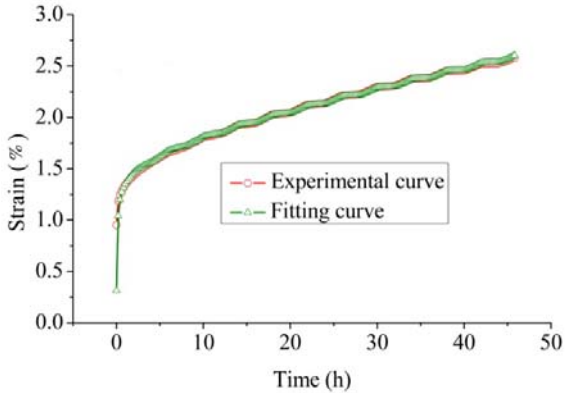

(a) SR1 sample

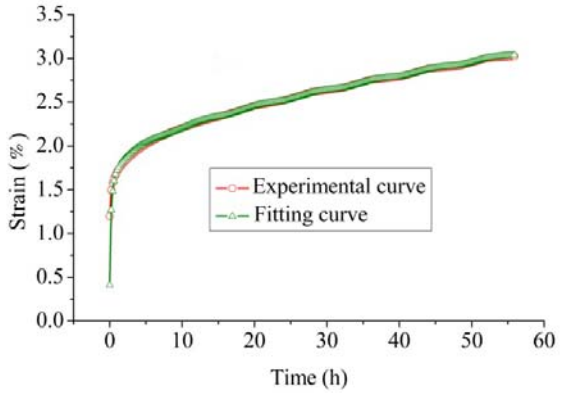

(b) SR2 sample

Fig. 6 Comparison of fitting and experimental creep curves: (a) SR1 sample; and (b) SR2 sample

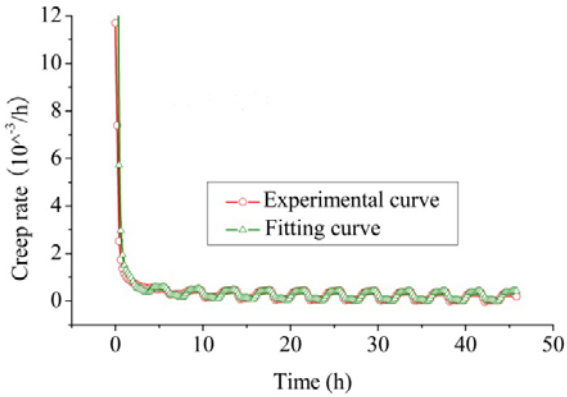

(a) SR1 sample

Fig. 7 Comparison of fitting and experimental creep rate curves: (a) SR1 sample; and (b) SR2 sample

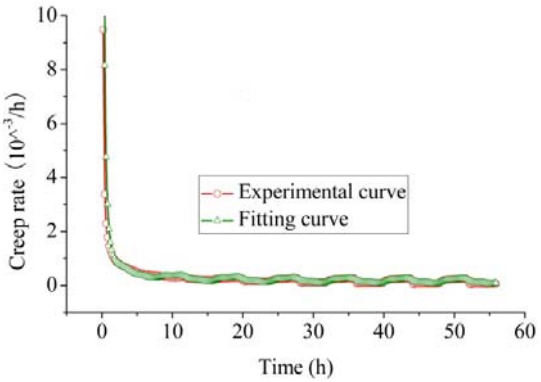

(b) SR2 sample

Fig. 7 Continued

the fitting curves are in excellent agreement with the experimental data. Thus, our model accurately reflects the creep property of salt rock under cyclic loading. In particular, it reflects distinct fluctuations in creep deformation and creep rate as the confining pressure increasing and decreasing under different cycle periods.

6. Conclusions

To investigate the creep behavior of salt rock under low-frequency cyclic loading, triaxial compression creep tests were performed on salt rock samples using cyclic confining pressure with a static axial pressure. The creep deformation properties of salt rock under low-frequency cyclic loading were then analyzed. A creep damage model for salt rock under low-frequency cyclic loading was established based on the rheology model and damage mechanics theories, and the suitability of which was evaluated using the test data.

- Salt rock samples exhibit significant time-dependent deformation. Up to a certain time (~6 h for sample SR1 and ~16 h for SR2), changes in the confining pressure have little influence on creep properties of salt rock, and the axial creep curve is smooth. After this point, changes in the confining pressure gradually affect the sample creep, and the axial creep curve clearly fluctuates with the confining pressure. The smaller the cycle period for the confining pressure is, the more distinct are the axial creep fluctuations. For the fluctuation stage, the creep curve is approximately a straight line both when the confining pressure decreases and when it increases within one cycle period. The slope of these lines differs: it is greater when the confining pressure decreases than when it increases. The creep rate curve exhibits a square wave pattern, with crests and troughs corresponding to decreasing and increasing confining pressure, respectively.
- In accordance with rheology model theory, axial creep equations were deduced for Maxwell and Kelvin models under cyclic loading. These were combined to establish an axial creep equation for the Burgers model. We supposed that damage evolution follows an exponential law during creep process and replaced the apparent stress in creep equation for the Burgers

model by the effective stress, the axial creep damage equation for the Burgers model was obtained.

- The model suitability was verified using creep test results for salt rock. The fitting curves are in excellent agreement with the test curves, so the proposed model can well reflect the creep behavior of salt rock under low-frequency cyclic loading. In particular, it reflects the fluctuations in creep deformation and creep rate as the confining pressure increasing and decreasing under different cycle periods.

As an attempt in the preliminary study, 2 samples were used for the creep test under low-frequency cyclic loading, and the creep damage model for salt rock under low-frequency cyclic loading was established based on the test results. However, due to the limited number of samples and small variation range of stress state, the creep damage model is applicable and acceptable in a limited range of stress conditions. In spite of the small number of samples, some useful conclusions can be made, and the basic pattern of the salt rock creep deformation under low-frequency cyclic loading is obtained, which provides an excellent foundation for the subsequent research. In the subsequent research, the authors will continue to work on this subject, use more samples with adjusted stress states for creep test, use more test data to verify the applicability and rationality of the model, and overcome its inadequacy.

Acknowledgments

The present work is subsidized and supported by the National Natural Science Foundation of China (51404184, 41202195). The financial supports are gratefully acknowledged by the authors!

References

Asanov, V.A. and Pan'kov, I.L. (2004), "Deformation of salt rock joints in time", *J. Min. Sci.*, **40**(4), 355-359.

Chan, K.S., Brodsky, N.S., Fossum, A.F., Bodner, S.R. and Munson, D.E. (1994), "Damage-induced nonassociated inelastic flow in rock salt", *Int. J. Plasticity*, **10**(6), 623-642.

Chan, K.S., Munson, D.E., Bodner, S.R. and Fossum, A.F. (1996), "Cleavage and creep fracture of rock salt", *Acta Mater.*, **44**(9), 3353-3365.

Chan, K.S., Bodner, S.R., Fossum, A.F. and Munson, D.E. (1997), "A damage mechanics treatment of creep failure in rock salt", *Int. J. Damage Mech.*, **6**(2), 121-152.

Chen, F., Yang, C.H. and Bai, S.W. (2007), "Investigation on optimized gas recovery velocity of natural gas storage in salt rock layer by numerical simulation", *Rock Soil Mech.*, **28**(1), 57-62. [In Chinese]

Chopra, P.N. (1997), "High-temperature transient creep in olivine rocks", *Tectonophysics*, **279**(1-4), 93-111.

Dubey, R.K. and Gairola, V.K. (2008), "Influence of structural anisotropy on creep of rock salt from Simla Himalaya, India: An experimental approach", *J. Struct. Geol.*, **30**(6), 710-718.

Guo, Y.T., Yang, C.H. and Mao, H.J. (2012), "Mechanical properties of Jintan mine rock salt under complex stress paths", *Int. J. Rock Mech. Min. Sci.*, **56**, 54-61.

Heusermann, S., Rolfs, O. and Schmidt, U. (2003), "Nonlinear finite-element analysis of solution mined storage caverns in rock salt using the LUBBY2 constitutive model", *Comput. Struct.*, **81**(8-11), 629-638.

Jiang, Y.Z., Xu, W.Y. and Wang, R.H. (2011), "Investigation on rheological mechanical properties of hornblende plagioclase gneiss", *Rock Soil Mech.*, **32**(Supp.1), 339-345. [In Chinese]

Jin, J. and Cristescu, N.D. (1998), "An elastic/viscoplastic model for transient creep of rock salt", *Int. J. Plasticity*, **14**(1-3), 85-107.

Lemaitre, J. (1984), "How to use damage mechanics", *Nucl. Eng. Des.*, **80**(2), 233-245.
Liang, W.G., Yang, C.H., Zhao, Y.S., Dusseault, M.B. and Liu, J. (2007), "Experimental investigation of mechanical properties of bedded salt rock", *Int. J. Rock Mech. Min. Sci.*, **44**(3), 400-411.
Liang, W.G., Zhao, Y.S., Xu, S.G. and Dusseault, M.B. (2011), "Effect of strain rate on the mechanical properties of salt rock", *Int. J. Rock Mech. Min. Sci.*, **48**(1), 161-167.
Munson, D.E. (1997), "Constitutive model of creep in rock salt applied to underground room closure", *Int. J. Rock Mech. Min. Sci.*, **34**(2), 233-247.
Nazary Moghadama, S., Mirzabozorg, H. and Noorzad, A. (2013), "Modeling time-dependent behavior of gas caverns in rock salt considering creep, dilatancy and failure", *Tunn. Undergr. Sp. Tech.*, **33**, 171-185.
Ślizowski, J. and Lankof, L. (2003), "Salt-mudstones and rock-salt suitabilities for radioactive-waste storage systems: rheological properties", *Appl. Energ.*, **75**(1-2), 137-144.
Wang, G.J., Guo, K.M., Christianson, M. and Konietzky, H. (2011), "Deformation characteristics of rock salt with mudstone interbeds surrounding gas and oil storage cavern", *Int. J. Rock Mech. Min. Sci.*, **48**(6), 871-877.
Wang, T.T., Yan, X.Z., Yang, H.L., Yang, X.J., Jiang, T.T. and Zhao, S. (2013), "A new shape design method of salt cavern used as underground gas storage", *Appl. Energ.*, **104**, 50-61.
Weidinger, P., Hampel, A., Blum, W. and Hunsche, U. (1997), "Creep behaviour of natural rock salt and its description with the composite model", *Mater. Sci. Eng. A*, **234-236**, 646-648.
Yahya, O.M.L., Aubertin, M. and Julien, M.R. (2000), "A unified representation of the plasticity, creep and relaxation behavior of rock salt", *Int. J. Rock Mech. Min. Sci.*, **37**(5), 787-800.
Yang, S.Q. and Cheng, L. (2011), "Non-stationary and nonlinear visco-elastic shear creep model for shale", *Int. J. Rock Mech. Min. Sci.*, **48**(6), 1011-1020.
Yang, C.H., Daemen, J.J.K. and Yin, J.H. (1999), "Experimental investigation of creep behavior of salt rock", *Int. J. Rock Mech. Min. Sci.*, **36**(2), 233-242.
Yang, C.H., Jing, W.J., Daemen, J.J.K., Zhang, G.M. and Du, C. (2013), "Analysis of major risks associated with hydrocarbon storage caverns in bedded salt rock", *Reliab. Eng. Syst. Safety*, **113**, 94-111.
Zhang, Z.L., Xu, W.Y. and Wang, W. (2011), "Study of Triaxial creep tests and its nonlinear visco-elastoplastic creep model of rock from compressive zone of dam foundation in Xiangjiaba hydropower station", *Chinese J. Rock Mech. Eng.*, **30**(1), 132-140. [In Chinese]
Zhang, H.B., Wang, Z.Y., Zheng, Y.L., Duan, P.J. and Ding, S.L. (2012), "Study on tri-axial creep experiment and constitutive relation of different rock salt", *Safety Sci.*, **50**(4), 801-805.
Zhou, H.W., Wang, C.P., Han, B.B. and Duan, Z.Q. (2011), "A creep constitutive model for salt rock based on fractional derivatives", *Int. J. Rock Mech. Min. Sci.*, **48**(1), 116-121.
Zhou, H.W., Wang, C.P., Duan, Z.Q., Zhang, M. and Liu, J.F. (2012), "Time-based fractional derivative approach to creep constitutive model of salt rock", *Scientia Sinica Physica, Mechanica & Astronomica*, **42**(3), 310-318. [In Chinese]
Zhou, H.W., Wang, C.P., Mishnaevsky Jr, L., Duan, Z.Q. and Ding, J.Y. (2013), "A fractional derivative approach to full creep regions in salt rock", *Mech. Time-Depend. Mater.*, **17**(3), 413-425.

CC